Journal of Sound and Vibration (2002) **252**(2), 370–384
doi:10.1006/jsvi.2001.3702, available online at http://www.idealibrary.com on IDEAL®

ON THE EIGENFREQUENCIES OF A TWO-PART BEAM–MASS SYSTEM

O. KOPMAZ AND S. TELLI

Department of Mechanical Engineering, College of Engineering and Architecture, Uludag University, Gorukle, Bursa 16059, *Turkey. E-mail: sevda@uludag.edu.tr*

(*Received* 13 *February* 2001, *and in final form* 18 *April* 2001)

1. INTRODUCTION

The free vibration of beams and rods carrying concentrated (lumped) or distributed mass has been extensively investigated in detail for the last three decades. To have an idea about the subject studied in the relevant literature one can refer to the papers listed at the end of this work. Among the vast number of papers, the following can be mentioned. Chen [1] and Goel [2] studied the eigenfrequencies of beams carrying a concentrated mass. Bhat and Wagner [3], and Bhat and Kulkarni [4] obtained the natural frequencies of a cantilevered beam with a slender tip mass. They showed that the gyroscopic effect of the tip mass on the frequencies must be taken into account when its dimensions are considerable compared with those of the carrying beam. Recently, Chan and Zhang [5] studied the free vibration of a cantilever tube partially filled with liquid, considering it as a beam with distributed mass. Chan *et al.* [6], and Chan and Wang [7] investigated the free vibration of simply supported and cantilever beams with distributed mass, using Euler–Bernoulli and Timoshenko beam models respectively. Chan *et al.* [8] treated the free vibration of a beam with two distributed masses in-span. Low [9] derived the frequency equations of a beam with a concentrated mass in-span under classical boundary conditions. Cutchins [10], Batan and Gürgöze [11] dealt with the longitudinal vibrations of rods carrying a concentrated mass. Gürgöze and and İnceoğlu [12] studied the axial vibration of an elastic rod with external distributed mass.

However, it is observed in these works that a system consisting of a mass carried by two different beam segments has not been treated yet. In this paper, a method is presented to obtain the natural frequencies of such a system as shown in Figure 1, due to its practical importance. The general frequency equation derived in the context of this method can also be used to find the eigenfrequencies of the beams either carrying or not carrying a concentrated mass, and non-uniform, two part beams. However, one should remember that the concept of rigidity is an idealization and a theoretical assumption which will not be valid at higher frequencies any more. Therefore, in order to establish a more realistic model for such a system, the intermediate mass must be considered a highly stiff portion of the entire system instead of assuming it ideally rigid.

2. MATHEMATICAL MODEL

In the system shown in Figure 1, it is assumed that the mass carried by two beam segments has a regular shape, symmetric with respect to its centre of gravity. The beam segments generally may posses different bending rigidity and density per unit length. In

0022-460X/02/$35.00

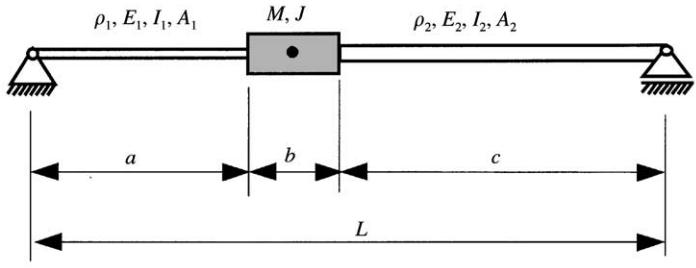

Figure 1. Two-part beam–mass system.

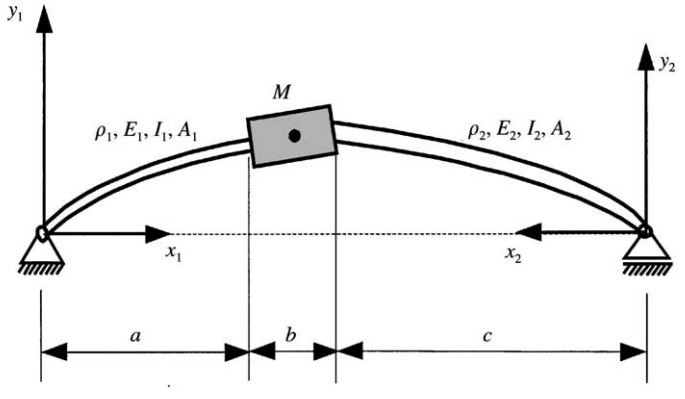

Figure 2. The deflected form of the two-part beam and the chosen co-ordinate systems.

Figure 2, a situation that the system may assume is shown exaggerated. At this stage of the study, the axial displacements are neglected because only the transversal vibrations are dealt with. The equations of motion of two beam segments will be derived in two different co-ordinate systems to express the boundary conditions on the right support more easily.

The segment with length a is enumerated with 1 whilst the other that has length c, with 2. In the $x_1 y_1$-co-ordinate system, the equation of motion of beam 1 will be

$$E_1 I_1 y_1'''' + \rho_1 A_1 \ddot{y}_1 = 0 \tag{1}$$

and that of beam 2 in $x_2 y_2$-co-ordinates

$$E_2 I_2 y_2'''' + \rho_2 A_2 \ddot{y}_2 = 0, \tag{2}$$

where ρ_i, E_i, A_i and I_i $(i = 1, 2)$ are the density, Young modulus, the cross-sectional area and area moment of inertia of each beam segment, respectively. The gyroscopic effect of the beam cross-sections is not accounted for. The primes $()'$ and the dots $\dot{()}$ denote the derivations with respect to x_1 or x_2, and time respectively.

2.1. BOUNDARY AND MATCHING CONDITIONS

In the $x_1 y_1$-co-ordinates the boundary conditions at the left end of beam 1 are

$$y_1(0, t) = 0, \tag{3}$$

$$E_1 I_1 y_1''(0, t) = 0, \tag{4}$$

whilst those at the right end of beam 2 in the $x_2 y_2$-co-ordinates are as follows:

$$y_2(0, t) = 0, \tag{5}$$

$$E_2 I_2 y_2''(0, t) = 0. \tag{6}$$

The total number of boundary conditions that beams 1 and 2 must satisfy at $x_1 = a$ and $x_2 = c$, respectively, is four. Two of them are the geometric boundary conditions and the remaining two the natural ones. In fact, it will be more meaningful to call these boundary conditions as matching or continuity conditions. These conditions are as follows:

$$y_1'(a, t) = - y_2'(c, t), \tag{7}$$

$$y_1(a, t) + b y_1'(a, t) = y_2(c, t), \tag{8}$$

$$E_1 I_1 y_1'''(a, t) + E_2 I_2 y_2'''(c, t) = M\left[\ddot{y}_1(a, t) + \frac{b}{2}\ddot{y}_1'(a, t)\right], \tag{9}$$

$$- E_1 I_1 y_1''(a, t) + E_2 I_2 y_2''(c, t) = J\ddot{y}_1'(a, t), \tag{10}$$

where M and J denote the amount of mass and the mass moment of inertia of the in-span attachment, respectively. Equations (7) and (8) are the geometrical matching conditions, and guarantee the continuity of the system. The natural or dynamic matching conditions given by equations (9) and (10) are, in fact, the equations of motion associated with the transverse displacement and rotation of the mass. When desired, the factors of M and J in equations (9) and (10) can be expressed in terms of the derivatives of y_2.

2.2. SOLUTION OF EQUATIONS OF MOTION

Based on the method of separation of variables, if the solutions for equations (1) and (2) are considered in the form

$$y_1(x_1, t) = Y_1(x_1) q(t), \tag{11}$$

$$y_2(x_2, t) = Y_2(x_2) q(t) \tag{12}$$

and substituted into those equations, after necessary rearrangements one finds

$$\frac{\ddot{q}}{q} = \frac{E_1 I_1 Y_1''''}{\rho_1 A_1 Y_1} = \frac{E_2 I_2 Y_2''''}{\rho_2 A_2 Y_2} = - \omega^2. \tag{13}$$

From equation (13), one arrives at the following:

$$Y_1'''' + k_1^4 Y_1 = 0, \tag{14}$$

$$Y_2'''' + k_2^4 Y_2 = 0. \tag{15}$$

Due to the existence of the relationship

$$\omega^2 = k_1^4 \frac{E_1 I_1}{\rho_1 A_1} = k_2^4 \frac{E_2 I_2}{\rho_2 A_2} \tag{16}$$

between ω^2, k_1, and k_2, it is concluded that the solutions of equations (14) and (15) will be as follows:

$$Y_1 = A_1 \cosh k_1 x_1 + B_1 \sinh k_1 x_1 + C_1 \cos k_1 x_1 + D_1 \sin k_1 x_1, \tag{17}$$

$$Y_2 = A_2 \cosh k_2 x_2 + B_2 \sinh k_2 x_2 + C_2 \cos k_2 x_2 + D_2 \sin k_2 x_2. \tag{18}$$

From equations (3)–(6), one obtains

$$A_1 = C_1 = A_2 = C_2 = 0. \tag{19}$$

Substituting Y_1 and Y_2 with the remaining terms into equations (7–10) yields a set of homogenous equations for B_1, D_1, B_2 and D_2. It is obvious that the determinant of the matrix of coefficients must vanish in order that these equations have non-trivial solutions. Equating the determinant to zero leads to the frequency equations of the system. Before providing the elements of this determinant, the definition of some non-dimensional parameters will be useful to generalize the results to be obtained. With

$$L = a + b + c \tag{20}$$

these parameters are defined as follows:

$$\frac{a}{L} = \eta_1, \qquad \frac{c}{L} = \eta_2, \qquad \frac{b}{L} = \eta_3 = (1 - \eta_1 - \eta_2), \tag{21–23}$$

$$\varphi = \frac{\rho_1 A_1}{\rho_2 A_2}, \qquad \xi = \frac{E_2 I_2}{E_1 I_1}. \tag{24, 25}$$

With the total mass of system segments

$$M_t = \rho_1 A_1 a + \rho_2 A_2 c, \tag{26}$$

the remaining non-dimensional parameters are introduced in the following manner:

$$\mu = \frac{M}{M_t}, \qquad \mu_1 = \frac{\rho_1 A_1 a}{M_t}, \qquad \mu_2 = \frac{\rho_2 A_2 c}{M_t}, \tag{27–29}$$

$$\lambda_1 = k_1 a, \qquad \lambda_2 = k_2 c, \qquad \psi = \frac{J}{M b^2}. \tag{30–32}$$

The elements of the (4×4) characteristic determinant d can be obtained using the aforementioned parameters as follows:

$$d_{11} = \lambda_1 \cosh \lambda_1, \qquad d_{12} = \lambda_1 \cos \lambda_1,$$

$$d_{13} = \frac{\eta_1}{\eta_2} \lambda_2 \cosh \lambda_2, \qquad d_{14} = \frac{\eta_1}{\eta_2} \lambda_2 \cos \lambda_2,$$

$$d_{21} = \sinh \lambda_1 + \left(\frac{1 - \eta_1 - \eta_2}{\eta_1} \right) \lambda_1 \cosh \lambda_1,$$

$$d_{22} = \sin \lambda_1 + \left(\frac{1 - \eta_1 - \eta_2}{\eta_1} \right) \lambda_1 \cos \lambda_1,$$

$$d_{23} = -\sinh \lambda_2, \qquad d_{24} = -\sin \lambda_2, \tag{33}$$

$$d_{31} = \lambda_1^3 \left[\cosh\lambda_1 + \mu \frac{(\eta_1 + \varphi\eta_2)}{\eta_1} \lambda_1 \sinh\lambda_1 + \frac{1}{2}\left(\frac{1-\eta_1-\eta_2}{\eta_1}\right)\mu\left(\frac{\eta_1+\varphi\eta_2}{\eta_1}\right)\lambda_1^2 \cosh\lambda_1 \right],$$

$$d_{32} = \lambda_1^3 \left[-\cos\lambda_1 + \mu \frac{(\eta_1 + \varphi\eta_2)}{\eta_1} \lambda_1 \sin\lambda_1 + \frac{1}{2}\left(\frac{1-\eta_1-\eta_2}{\eta_1}\right)\mu\left(\frac{\eta_1+\varphi\eta_2}{\eta_1}\right)\lambda_1^2 \cos\lambda_1 \right],$$

$$d_{33} = \xi\left(\frac{\eta_1}{\eta_2}\right)^3 \lambda_2^3 \cosh\lambda_2, \qquad d_{34} = -\xi\left(\frac{\eta_1}{\eta_2}\right)^3 \lambda_2^3 \cos\lambda_2,$$

$$d_{41} = \lambda_1^2 \left[-\sinh\lambda_1 + \psi\mu \frac{(\eta_1 + \varphi\eta_2)(1-\eta_1-\eta_2)^2}{\eta_1^3} \lambda_1^3 \cosh\lambda_1 \right],$$

$$d_{42} = \lambda_1^2 \left[\sin\lambda_1 + \psi\mu \frac{(\eta_1 + \varphi\eta_2)(1-\eta_1-\eta_2)^2}{\eta_1^3} \lambda_1^3 \cos\lambda_1 \right],$$

$$d_{43} = \xi\left(\frac{\eta_1}{\eta_2}\right)^2 \lambda_2^2 \sinh\lambda_2, \qquad d_{44} = -\xi\left(\frac{\eta_1}{\eta_2}\right)^2 \lambda_2^2 \sin\lambda_2.$$

Then, the characteristic equation is given by

$$\begin{vmatrix} d_{11} & d_{12} & d_{13} & d_{14} \\ d_{21} & d_{22} & d_{23} & d_{24} \\ d_{31} & d_{32} & d_{33} & d_{34} \\ d_{41} & d_{42} & d_{43} & d_{44} \end{vmatrix} = 0. \tag{34}$$

To approximately obtain the fundamental frequency of the system studied here by a different way the mathematical expression of the deflection curve related to the two-part beam–mass model (TPBMM) was derived. Since the beam segments have different geometry and material, their slopes and deflections are different from each other. The slopes and deflections of beam segments 1 and 2 are shown by the symbols y_1', y_2', y_1 and y_2 respectively. The slope and deflection expressions of both segments are non-dimensionalized in a suitable manner. With the non-dimensional slopes and deflections $\bar{y}_1'$, $\bar{y}_2'$, $\bar{y}$ and $\bar{y}_2$, the relationships used to non-dimensionalize them are as follows:

$$y_1' = \frac{G_T L^2}{E_1 I_1} \bar{y}_1', \qquad y_1 = \frac{G_T L^3}{E_1 I_1} \bar{y}_1, \tag{35, 36}$$

$$y_2' = \frac{G_T L^2}{E_2 I_2} \bar{y}_2', \qquad y_2 = \frac{G_T L^3}{E_2 I_2} \bar{y}_2, \tag{37, 38}$$

where G_T denotes the total weight of the system. If the bending stiffnesses of the beam segments are the same, the non-dimensionalizing factors also will be the same, $\bar{R}_1$ and $\bar{R}_2$ are the non-dimensional reaction forces at the left and right supports, which are obtained by dividing the actual reactions by G_T, and they are as follows:

$$\bar{R}_1 = \mu_1\left(1 - \frac{\eta_1}{2}\right) + \mu_2 \frac{\eta_2}{2} + \mu\left[\frac{1-(\eta_1-\eta_2)}{2}\right], \tag{39}$$

$$\bar{R}_2 = \mu_1 \frac{\eta_1}{2} + \mu_2\left(1 - \frac{\eta_2}{2}\right) + \mu\left[\frac{1+(\eta_1-\eta_2)}{2}\right]. \tag{40}$$

The non-dimensional slope and deflection functions were found as is given in the following:

$$\bar{y}_1' = \frac{\bar{R}_1}{2}\bar{x}_1^2 - \frac{1}{6}\frac{\mu_1}{\eta_1}\bar{x}_1^3 + \frac{1}{\xi}\left(\frac{1}{2}\eta_2 f_1 + \frac{1}{6}f_2\right), \quad \eta_1 \geqslant \bar{x}_1 \geqslant 0, \tag{41}$$

$$\bar{y}_1 = \frac{\bar{R}_1}{6}\bar{x}_1^3 - \frac{1}{24}\frac{\mu_1}{\eta_1}\bar{x}_1^4 + \frac{1}{\xi}\left(\frac{1}{2}\eta_2 f_1 + \frac{1}{6}f_2\right)\bar{x}_1, \tag{42}$$

$$\bar{y}_2' = \frac{\bar{R}_2}{2}\bar{x}_2^2 - \frac{1}{6}\frac{\mu_2}{\eta_2}\bar{x}_2^4 + \left(\frac{1}{2}(1-\eta_2)f_1\frac{1}{6}f_2\right), \quad \eta_2 \geqslant \bar{x}_2 \geqslant 0 \tag{43}$$

$$\bar{y}_2 = \frac{\bar{R}_2}{6}\bar{x}_2^3 - \frac{1}{24}\frac{\mu_2}{\eta_2}\bar{x}_2^4 + \left(\frac{1}{2}(1-\eta_2)f_1\frac{1}{6}f_2\right)\bar{x}_2, \tag{44}$$

where

$$\bar{x}_1 = \frac{x_1}{L}, \qquad \bar{x}_2 = \frac{x_2}{L}, \tag{45, 46}$$

$$f_1 = \mu_1\left[(\xi\eta_1^2 - \eta_2^2)\frac{\eta_1}{2} - \frac{2}{3}\xi\eta_1^2\right] + \mu_2\left[-(\xi\eta_1^2 - \eta_2^2)\frac{\eta_2}{2} - \frac{2}{3}\eta_2^2\right]$$
$$+ \mu\left[-(\xi\eta_1 + \eta_2)\eta_1\eta_2 - (\xi\eta_1^2 + \eta_2^2)\frac{(1-\eta_1-\eta_2)}{2}\right], \tag{47}$$

$$f_2 = \mu_1\left[-\xi\eta_1^3\left(-\frac{1}{2} + \eta_1 + \frac{3}{2}\eta_2 + 2\frac{(1-\eta_1-\eta_2)}{\eta_1}\right) + \eta_2^3\frac{\eta_1}{2}\right]$$
$$+ \mu_2\left[-\xi\eta_1^3\left(1 + 3\frac{(1-\eta_1-\eta_2)}{\eta_1}\right)\frac{\eta_2}{2} + \eta_2^3\left(\frac{3}{4} - \frac{\eta_2}{2}\right)\right]$$
$$+ \mu\left[-\xi\eta_1^3\left(1 + 3\frac{(1-\eta_1-\eta_2)}{\eta_1}\right)\frac{(1-\eta_1+\eta_2)}{2} + \eta_2^3\frac{(1+\eta_1-\eta_2)}{2}\right]. \tag{48}$$

The non-dimensional deflection of the mass M was obtained as follows:

$$\bar{y}_m = \mu_1\left[\left(\frac{1}{6}\eta_1^3 + \frac{1}{4}\eta_1^2(1-\eta_1-\eta_2)\right)\left(1 - \frac{\eta_1}{2}\right) - \frac{1}{24}\eta_1^3 - \frac{1}{12}\eta_1^2\eta_3\right]$$
$$+ \mu_2\left[\left(\frac{1}{6}\eta_1^3 + \frac{1}{4}\eta_1^2(1-\eta_1-\eta_2)\right)\frac{\eta_1}{2}\right]$$
$$+ \mu\left[\left(\frac{1}{6}\eta_1^3 + \frac{1}{4}\eta_1^2(1-\eta_1-\eta_2)\right)\left(\frac{1-\eta_1+\eta_2}{2}\right)\right]$$
$$+ \frac{1}{\xi}\left(\frac{1}{2}\eta_2 f_1 + \frac{1}{6}f_2\right)\left(\frac{1+\eta_1-\eta_2}{2}\right). \tag{49}$$

The relationship between the dimensional and non-dimensional deflections of the mass y_m and $\bar{y}_m$ is defined as

$$y_m = \frac{G_T L^3}{E_1 I_1}\bar{y}_m. \tag{50}$$

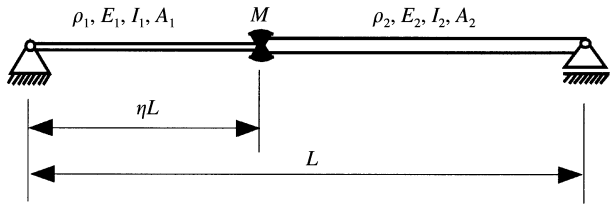

Figure 3. Beam with concentrated mass.

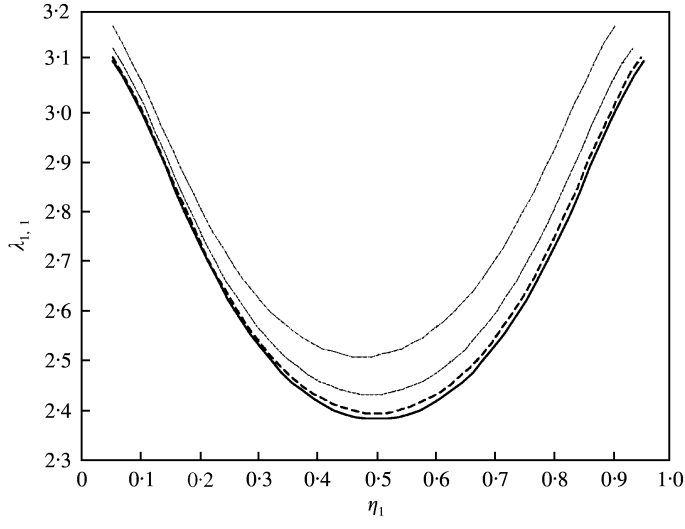

Figure 4. The variation of the first frequency according to the BCMM and TPCMM with respect to η and η_1 respectively. ——, BCMM; - - - -, TPBMM ($\eta_3 = 0{\cdot}005$); – – – –, TPBMM ($\eta_3 = 0{\cdot}02$); – · – · –, TPBMM ($\eta_3 = 0{\cdot}05$).

3. NUMERICAL RESULTS

To obtain the roots of the characteristic equation given by equation (34), a MATLAB-code was written (although the roots of this equation are, in fact, the eigenvalues of the system, we prefer to use the term frequency or eigenfrequency for convenience, based on the relationship between these two entries). The mathematical model established in this work allows one to find the bending eigenfrequencies of stepped beams and shafts, beams of continuous cross-section, and beams carrying a concentrated mass. For the purpose of comparison, another model was developed considering the physical system shown in Figure 3. These two models will be briefly denoted with the abbreviations TPBMM (two-part beam–mass model) and BCMM (beam with concentrated mass model).

By means of the TPBMM, the effects of some non-dimensional parameters on the frequencies were investigated. In what follows, the numerical results presented graphically for different cases will be interpreted and some comments will be made.

With μ and b/L held constant, it was investigated how the first three frequencies vary with respect to η_1 that can be considered as non-dimensional length of beam 1, or as the connection point of mass M. (The distance of the centre of gravity of the mass from the left support might be utilized as a variable instead of η_1. However, since η_1 seems to be more meaningful and easy to imagine, it was preferred.) In Figures 4–6, the curves with solid line

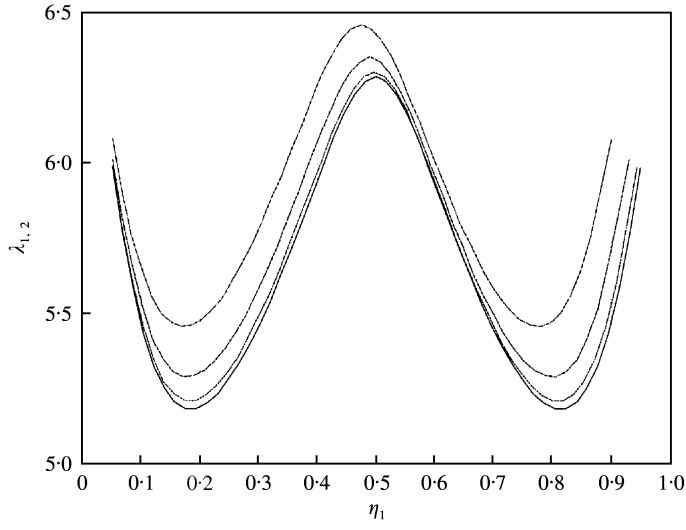

Figure 5. The variation of the second frequency according to the BCMM and TPCMM with respect to η and η_1 respectively. ——, BCMM; - - - -, TPBMM ($\eta_3 = 0{\cdot}005$); – – – –, TPBMM ($\eta_3 = 0{\cdot}02$); – · – · – ·, TPBMM ($\eta_3 = 0{\cdot}05$).

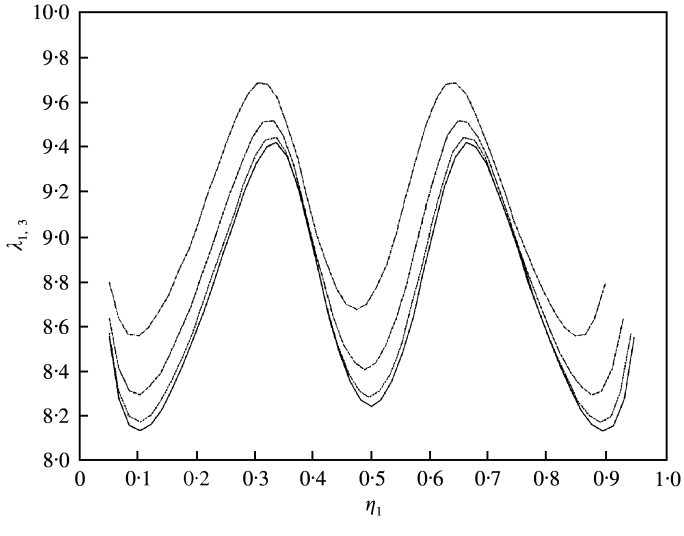

Figure 6. The variation of the third frequency according to the BCMM and TPCMM with respect to η and η_1 respectively. ——, BCMM; - - - -, TPBMM ($\eta_3 = 0{\cdot}005$); – – – –, TPBMM ($\eta_3 = 0{\cdot}02$); – · – · – ·, TPBMM ($\eta_3 = 0{\cdot}05$).

are obtained from the BCMM. All these curves were obtained for $\mu = 0{\cdot}5$, $\varphi = \xi = 1$, and $\psi = 0$. In the TPBMM, different curves corresponding to different values of b/L were plotted. These values of b/L are 0·005, 0·02 and 0·05 respectively. The horizontal axis in the figures represents η_1 for the TPBMM, and η for the BCMM. To make a direct comparison between the results of both models, the values λ_1 found from the TPBMM were divided by η_1. From these figures, the following conclusions can be drawn.

The frequency curves related to the BCMM are always below those obtained from the TPBMM. When the ratio b/L increases for a constant μ, some increase in the mass of beam

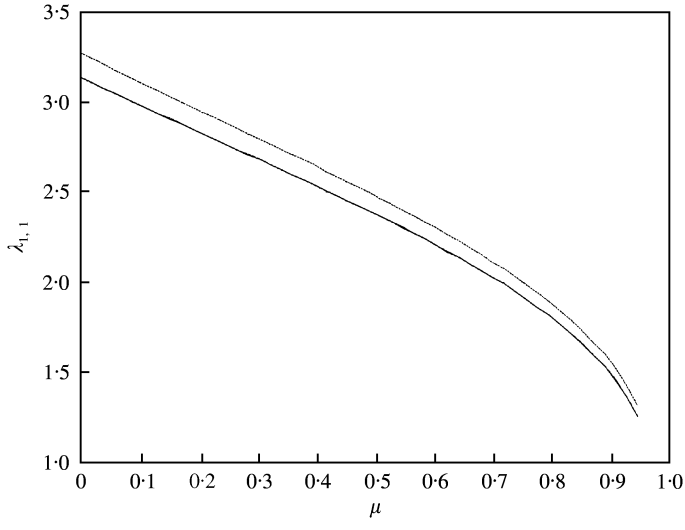

Figure 7. The variation of the first frequency according to the BCMM and TPCMM with respect to μ. ----, TPBMM ($\eta_1 = 0{\cdot}50$); ——, BCMM ($\eta = 0{\cdot}48$); –·–·–, BCMM ($\eta = 0{\cdot}50$).

segments must be expected in order to keep μ constant. Since $\varphi = \xi = 1$, this is possible if only the beam cross-section gets larger. As a consequence, the beam segments become stiffer, thus the frequencies have higher values.

Another remarkable point in these figures is that the second and third frequency curves have the extrema of certain numbers. The second frequency has one maximum, two minima, while the third one has two maxima and three minima. These extrema correspond to the nodes and anti-nodes of the associated modes [13]. The minima and maxima approximately indicate the locations of anti-nodes and nodes respectively. Hence, the curve of first frequency has just one anti-node, while the second has one node, two anti-nodes, and the third one has two nodes, three anti-nodes. From this observation, it is easily concluded that the system studied here has modes resembling those of a simply supported beam.

Figures 7–9 show how the first three frequencies vary with η_1 provided that η_1, η_2 (moreover $\eta_1 = \eta_2$) and thus $b/L = 1 - \eta_1 - \eta_2$ are held constant. Furthermore, some parameters for the TPBMM were chosen as $\eta_1 = \eta_2 = 0{\cdot}48$, $b/L = 1 - \eta_1 - \eta_2 = 0{\cdot}04$, $\varphi = \xi = 1$. In all figures the dotted curves belong to the TPBMM whilst the dashed and solid curves represent the results obtained from the BCMM for $\eta = 0{\cdot}5$ and $0{\cdot}48$ respectively. So two different comparisons can be made using these figures. The frequency curves related to the BCMM for $\eta = 0{\cdot}5$ change similar to, but below those of the TPBMM. Keeping the dimensions of the beam segments same, it is possible to alter μ in the BCMM contrary to the TPBMM in which changing μ has an indirect effect on the beam dimensions. Consequently, the stiffness does not change in the BCMM even if μ increases, which causes a decrease in the first frequency, while the TPBMM has a higher frequency value because an increase in μ leads to a rise in the systems stiffness, Figure 7. Although the first frequency curves of the BCMM corresponding to $\eta = 0{\cdot}50$ and $0{\cdot}48$ are not distinguishable in the graphics, the curve for $\eta = 0{\cdot}50$ goes below the curve for $\eta = 0{\cdot}48$. This situation can be explained in the manner that the location of the mass M coincides with an anti-node for $\eta = 0{\cdot}50$ and hence the system has more kinetic energy than the case for $\eta = 0{\cdot}48$. When the second frequency curves are considered, it draws attention to the fact that the curve of the TPBMM and that of the BCMM for $\eta = 0{\cdot}50$ appear not to be

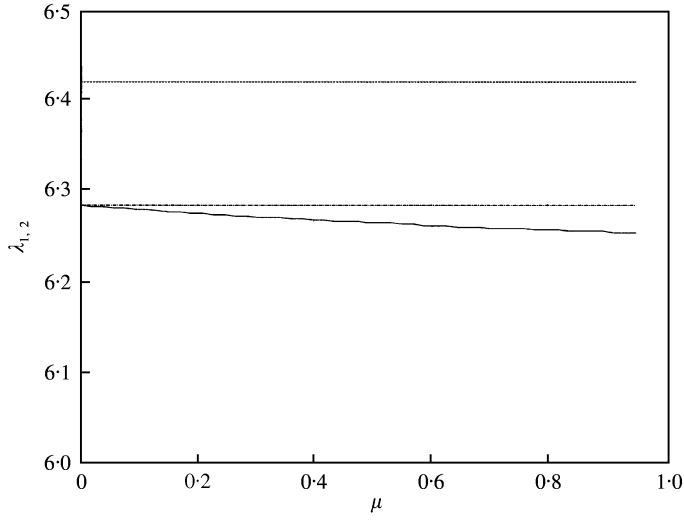

Figure 8. The variation of the second frequency according to the BCMM and TPCMM with respect to μ. ----, TPBMM ($\eta_1 = 0{\cdot}50$); ——, BCMM ($\eta = 0{\cdot}48$); –·–·–, BCMM ($\eta = 0{\cdot}50$).

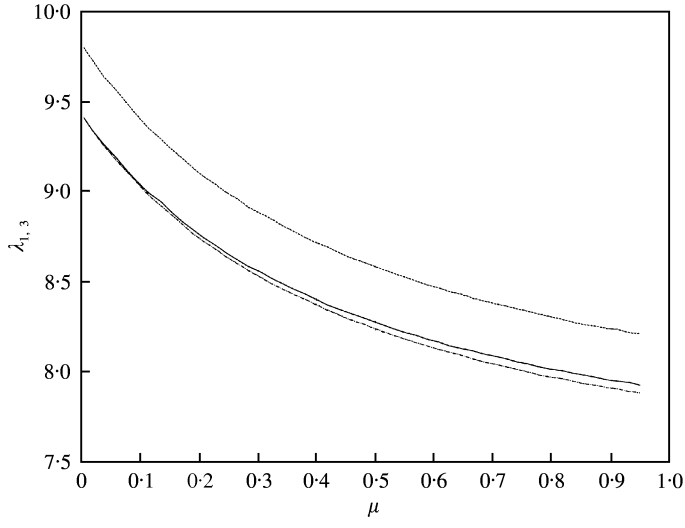

Figure 9. The variation of the third frequency according to the BCMM and TPCMM with respect to μ. ----, TPBMM ($\eta_1 = 0{\cdot}50$); ——, BCMM ($\eta = 0{\cdot}48$); –·–·–, BCMM ($\eta = 0{\cdot}50$).

sensitive to the change in μ. This also implies that the mass is located in the neighbourhood of or on a node, for both models. From this observation, it is concluded that there is a node in the middle of beam span in each system. In the same figure, one sees that the second frequency of the BCMM for $\eta = 0{\cdot}48$ varies with μ, because in this case the mass is not on a node. Moreover, the frequency decreases with increase in μ. If the Rayleigh quotient is recalled, this phenomenon will be easily understood. The reference kinetic energy in the denominator of this quotient gets greater, which leads to a decrease in the second frequency. In Figure 9, similar curves for the third frequency are plotted. The curve related to the

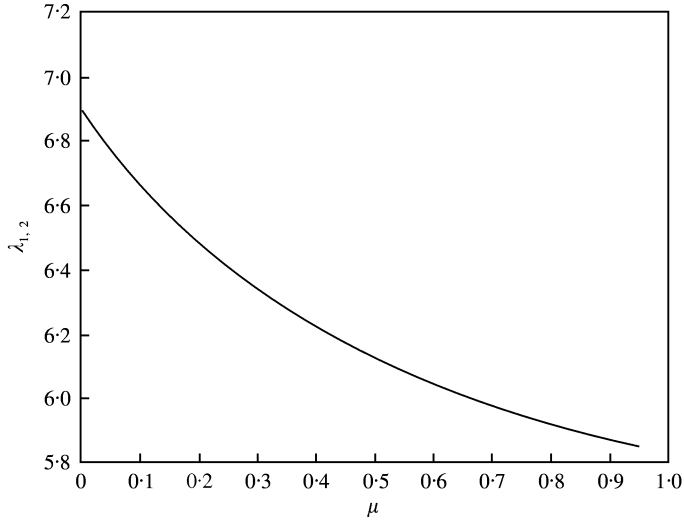

Figure 10. The second frequency versus μ in case the mass is not located on a node.

TPBMM again lies above those of the BCMM due to the aforementioned reasons. Contrary to the second frequency, here, the curve of the BCMM for $\eta = 0{\cdot}48$ goes above the curve for $\eta = 0{\cdot}50$. This can be explained by means of modes. In the case of $\eta = 0{\cdot}50$, the mass is placed on the anti-node of the associated mode. Since the non-dimensional distance $\eta = 0{\cdot}48$ is slightly far away from the anti-node, the reference kinetic energy corresponding to $\eta = 0{\cdot}50$ is greater, and hence the frequency becomes smaller.

To check whether the explanation for the second frequency is reasonable, by taking $\eta_1 = 0{\cdot}6$, $\eta_2 = 0{\cdot}3$, $\varphi = \xi = 1$ and $\psi = 0$, a new curve for the second frequency was obtained from the TPBMM, and it was observed that the second one varies with μ, when the mass M is not on a node, Figure 10.

Figure 11 shows how the values of the first frequency obtained from the TPBMM and an approximate formula similar to Dunkerley's formula change with respect to μ. Here, the location of the mass M does not alter, and according to the relationship $\eta_1 + (1 - \eta_1 - \eta_2)/2 = 0{\cdot}6 + (1 - 0{\cdot}6 - 0{\cdot}3)/2 = 0{\cdot}65$, it is at $0.65L$. In this approximate method, the deflection of the mass centre is obtained by equation (49), and the first frequency is calculated by the formula $\omega_1 \cong (g/y_m)^{1/2}$. The difference between this formula and Dunkerley's approximation is that, Dunkerley's method finds two separate frequencies based on the weights of beam and mass, then calculates the first frequency by using these two. However, in the method used here, the weights of beam segments are included in the calculation of the deflection y_m. In this approximate method, the numeric values of the geometric and physical parameters were chosen as follows.

For the beam segments (*assumed uniform and homogenous*): $E = 2.1 \times 10^{11}$ N/m^2, $\rho = 7850$ kg/m^3, $L = 1$ m, $a = 0{\cdot}6$ m, $b = 0{\cdot}1$ m, $c = 0{\cdot}3$ m, D (beam diameters) $= 0{\cdot}2$ m. In this example, the lengths of beam segments are kept constant, and μ is altered by increasing M.

In Figures 12 and 13, the variation of the first and second frequencies over η_1 is given for different values of φ. Here, it was assumed that two beam segments are made from the same material, and accordingly, it is taken that $\xi = \varphi^2$. For both graphics $\mu = 0{\cdot}5$.

In Figure 12, it is observed that the first frequency rises as φ increases. An increase in φ means a larger diameter of the beam segment 2. The minima of each of the three curves

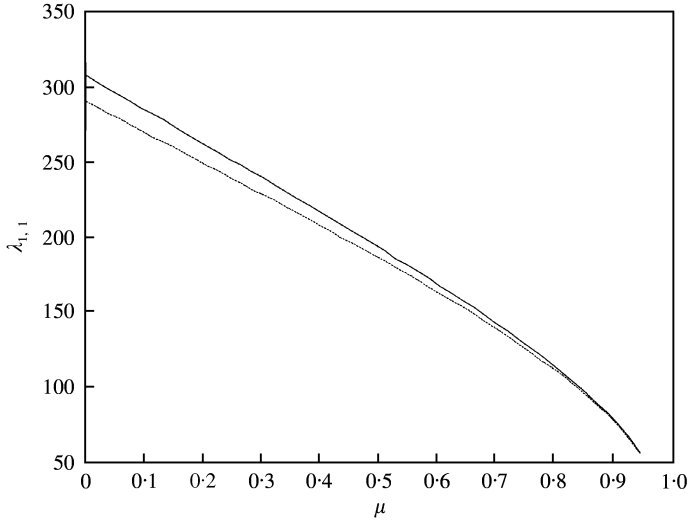

Figure 11. The variation of the first frequency according to the BCMM and approximate method with respect to μ. ——, TPBMM; - - - - -, approximate method.

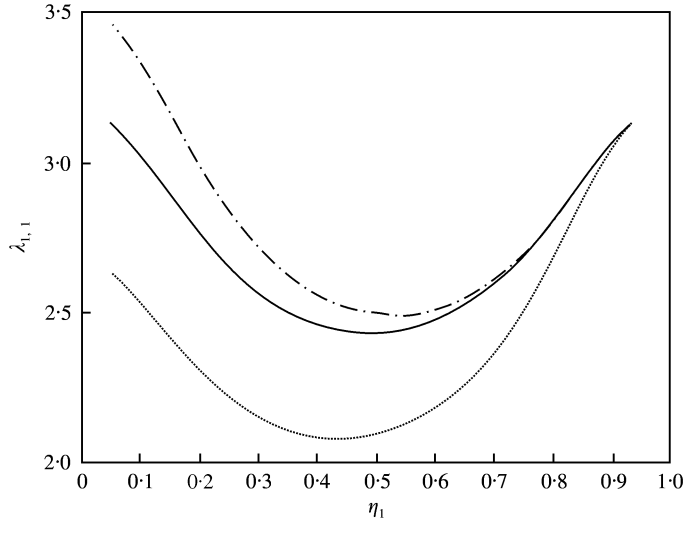

Figure 12. The variation of the first frequency according to the TPBMM for different values of φ. - - - -, $\varphi = 0{\cdot}5$; ——, $\varphi = 1$; –·–·–, $\varphi = 1{\cdot}5$.

correspond to the anti-node of the first mode for every φ. For $\varphi = 1{\cdot}5$, $\eta_1 < 0{\cdot}5$ the slimmer segment 1 becomes shorter (in other words, the length of segment 2 increases), and thus the system stiffness increases along with higher φ values. For this reason, the curve $\varphi = 1{\cdot}5$ is above that for $\varphi = 1$, and the last one is above the curve for $\varphi = 0{\cdot}5$. When η_1 approaches 1, it is observed that all the curves get closer. This is an expected consequence because the contribution of segment 2 to the system stiffness decreases. There is a similar situation for the curves related to the second frequency shown in Figure 13.

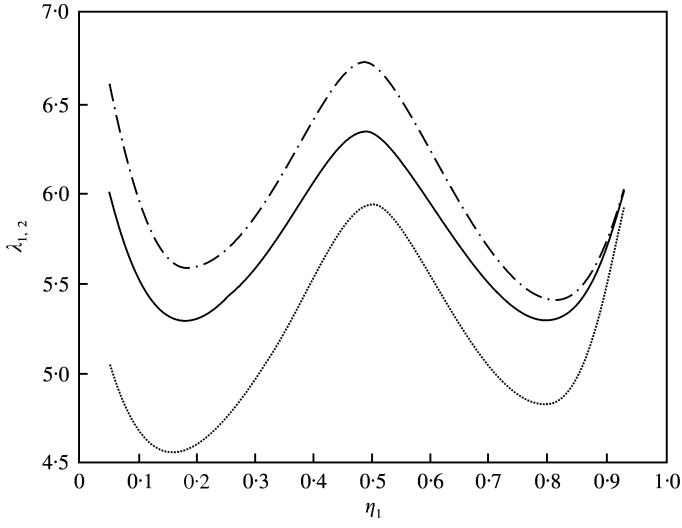

Figure 13. The variation of the second frequency according to the TPBMM for different values of φ. ----, $\varphi = 0{\cdot}5$; ——, $\varphi = 1$; –·–·–, $\varphi = 1{\cdot}5$.

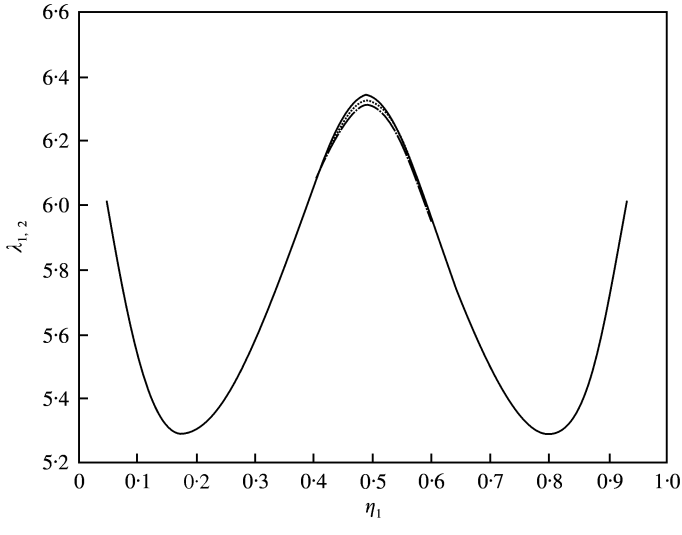

Figure 14. The variation of the second frequency according to the TPBMM with respect to η_1 for different values of ψ. ——, $\psi = 0$; -----, $\psi = 0{\cdot}10$; -----, $\psi = 0{\cdot}16$; –·–·–, $\psi = 0{\cdot}41$.

In Figures 14 and 15, the variations of the second and third frequencies with η_1, including the gyroscopic effect of the mass M, are shown. Note that $\mu = 0{\cdot}5$, $b/L = 0{\cdot}02$ for these curves. The smaller the value of ψ, the higher are the frequencies. Since the curves of the first frequency for different ψ's appear as if they are coincident within the scale of graphics, it is not given here. With increasing order of the frequencies the variation with ψ becomes more distinguishable. This observation is in good agreement with classical vibration theory, which states that the gyroscopic effect is dominant at higher frequencies. From these last

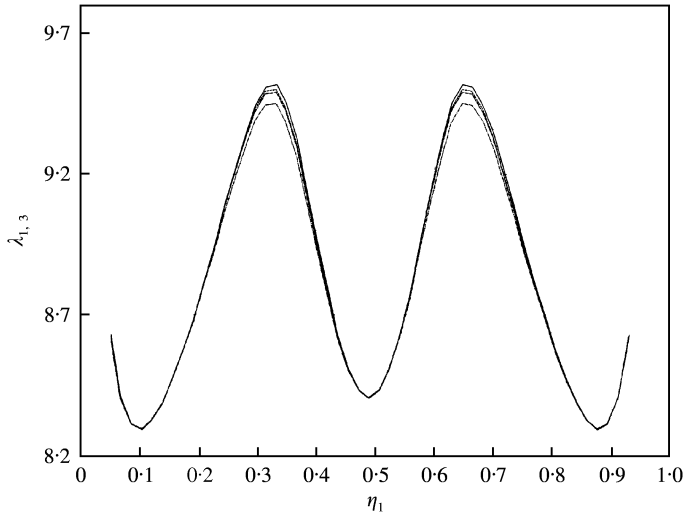

Figure 15. The variation of the third frequency according to the TPBMM with respect to η_1 for different values of ψ. ——, $\psi = 0$; - - - - -, $\psi = 0{\cdot}10$; – – –, $\psi = 0{\cdot}16$; – · – · –, $\psi = 0{\cdot}41$.

analyses one sees that ψ does not influence the first three frequencies. Consequently, it is understood that taking $\psi = 0$ for other case studies is reasonable.

4. CONCLUSIONS

In this study, a mathematical model is presented to obtain the bending frequencies of a system which consists of two beam segments carrying a mass of considerable dimensions. This model allows one to investigate some special cases such as stepped beams and shafts, uniform and homogenous beams, and beams carrying a concentrated mass. Since the mass in the model forms a region with no flexibility on the system, this model is not suitable to study elastic systems carrying distributed mass. In this model the material and geometric properties of the beam segments can be controlled via the parameters φ and ξ.

Another significant point to mention is that the equation of motion and characteristic equation are derived by using two different co-ordinate systems. So, a useful model that enables one to study stepped beams and shafts, is established. That the equation of the elastic curve related to this system was derived in a non-dimensional form is among the original contributions of this work.

REFERENCES

1. Y. CHEN 1963 *American Society of Mechanical Engineers Journal of Applied Mechanics* **30**(2), 310–312. On the vibration of beams or rods carrying a concentrated mass.
2. R. P. GOEL 1973 *American Society of Mechanical Engineers Journal of Applied Mechanics* **40**(3), 821–822. Vibrations of a beam carrying a concentrated mass.
3. B. R. BHAT and H. WAGNER 1976 *Journal of Sound and Vibration* **45**, 304–307. Natural frequencies of a uniform cantilever with a tip mass slender in the axial direction.
4. R. BHAT and M. A. KULKARNI 1976 *American Institute of Aeronautics and Astronautics Journal* **14**, 536–537. Natural frequencies of a cantilever with slender tip mass.
5. K.-T. CHAN and J.-Z. ZHANG 1995 *Journal of Sound and Vibration* **182**, 185–190. Free vibration of a cantilever tube partially filled with liquid.

6. K.-T. CHAN, T.-P. LEUNG and W. O. WONG 1996 *Journal of Sound and Vibration* **191**, 590–597. Free vibrations of simply supported beam partially loaded with distributed mass.
7. K.-T. CHAN and X.-Q. WANG 1997 *Journal of Sound and Vibration* **206**, 353–369. Free vibration of a Timoshenko beam partially loaded with distributed mass.
8. K.-T. CHAN, X.-Q. WANG and T.-P. LEUNG 1998 *American Society of Mechanical Engineers Journal of Vibration and Acoustics* **120**, 944–948. Free vibrations of beams with two sections of distributed mass.
9. K. H. LOW 1998 *Journal of Sound and Vibration* **215**, 381–389. On the eigenfrequencies for mass loaded beams under classical boundary conditions.
10. M. A. CUTCHINS 1980 *Journal of Sound and Vibration* **73**, 185–193. The effect of an arbitrarily located mass on the longitudinal vibrations of a bar.
11. H. BATAN and M. GÜRGÖZE 1996 *Journal of Sound and Vibration* **194**, 751–756. On the effect of an arbitrarily located mass on the longitudinal vibrations of a bar.
12. M. GÜRGÖZE and S. İNCEOĞLU 2000 *Journal of Sound and Vibration* **230**, 187–194. On the vibrations of an axially vibrating elastic rod with distributed mass added in-span.
13. P. D. CHA and C. L. DYM 1998 *Journal of Sound and Vibration* **211**, 249–264. Identifying nodes and anti-nodes of complex structures with virtual elements.